NTNU – Trondheim
Norwegian University of
Science and Technology

Investigation of Interior Permanent Magnet Machines with Concentrated Windings for High Dynamics Applications

Christian Svihus

Master of Energy and Environmental Engineering
Submission date: June 2015
Supervisor: Robert Nilssen, ELKRAFT
Co-supervisor: Arne Nysveen, ELKRAFT

Norwegian University of Science and Technology
Department of Electric Power Engineering

Investigation of Interior Permanent Magnet Machines with Concentrated Windings for High Dynamics Applications

Christian Svihus
Department of Electrical Engineering
Norwegian University of Science and Technology (NTNU)
Trondheim, June 2015

***Abstract*—Interior permanent magnet (IPM) machines and non-overlapping concentrated windings (CW) are two permanent magnet machine design philosophies that have grown in popularity over the last couple of decades. This is due to many benefits and the flexibility they provide. The combination of these philosophies and the tradeoffs involved, however, have not yet been fully discovered. The hope is that the performance enhancing properties of the IPM can be combined with the manufacturability of the CW.**

An investigation of these two philosophies have been done, focusing on torque performances and magnet losses caused by eddy currents. In order to do the investigation the finite element method (FEM) analysis software, COMSOL Multiphysics have been used. Two IPM models have been compared to a surface mounted permanent magnet (SPM) machine using the same stator design and winding philosophies.

The IPM machines showed capability of reaching approximately the same average torque as the SPM machine, although performing poorly when considering torque ripple performance. Considering magnet losses, the IPM machines showed little tendency to reduce the full-load magnet losses. No-load losses, however, was drastically reduced in the IPM models compared to the SPM model. The effect of magnet segmentation on magnet losses was also demonstrated.

I. Introduction

PERMANENT magnet (PM) machines are being utilised in an increasingly wider range of applications. Characterised by increased efficiency and performance they are becoming more and more popular. Where synchronous machines with field windings and induction machines previously have had sovereignty, PM machines are now being used. The field of usage spans from wrist watches to marine propulsion systems. There are several ways to implement permanent magnets in electrical machines. The *interior permanent magnet machine (IPM)* is thought to achieve increased efficiency and several other benefits. Design-wise, the permanent magnets in the IPM are incorporated in the rotor structure, contrary to the more commonly used surface mounted permanent magnet rotor (SPM), In the SPM the magnets are glued or attached to the rotor surface. From theoretical assumptions and early studies the key benefits of IPM machines are:

- Improved mechanical ruggedness of the rotor
- Increased torque due to rotor saliency
- Simpler implementation of sensor-less control
- Reduced risk of demagnetisation due to magnetic shielding of the magnets
- Great flux-weakening capabilities
- Opportunity to use rectangular magnets

  [4], [5]

These advantages have resulted in more research work on IPMs which has further lead to implementation in industry. This have primarily been associated with traction appliances. This is due to the IPM's much appreciated properties, where its wide constant power speed range [5] being the most important one. However the overall benefits suggests a much broader range of use.

Non-overlapping concentrated stator windings (CW) presents a significant increase in manufacturability of the stator. The coils can, in most cases, be wound prior to assembly of the stator, allowing for an automated, and thus cost-reducing, assembly process. It also facilitates an increased slot fill factor [20]. Earlier it was believed that the CW could not match the performance of the more commonly used distributed overlapping winding (DW). But Cros and Viarouge [10] and Magnussen and Sadarangani [11] discovered that by an appropriate slot-pole combination, the CW could perform equal to the DW. Following these results, the research activity on this type of winding configuration have increased.

However, as stated in the work of El-Refaie [20], the *combination* of CW and IPM is not mature, and there are still a lot of research to be done. The hope is that the best of both worlds may be utilised.

Following the IT revolution that has taken place the last two decades, the computational power and software development have had a great impact on industrial design and optimisation processes. Finite element method (FEM) softwares like COMSOL Multiphysics, have shown to be particularly flexible, reliable and effective tools in testing theories and optimise designs. It is able to couple multiple physics and solving partial differential equations associated with the problems in question. It is also ideal for simplifying and isolating different areas of interest in order to gain a deeper understanding of design solutions. COMSOL Multiphysics is used extensively throughout the work in this thesis, and have been the main source of results.

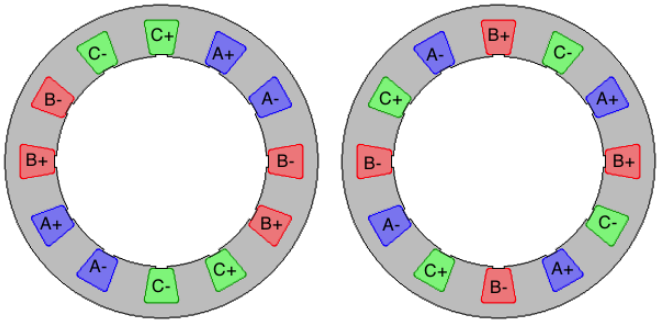

(a) Concentrated winding (b) Distributed winding

Figure 1: Winding orientation

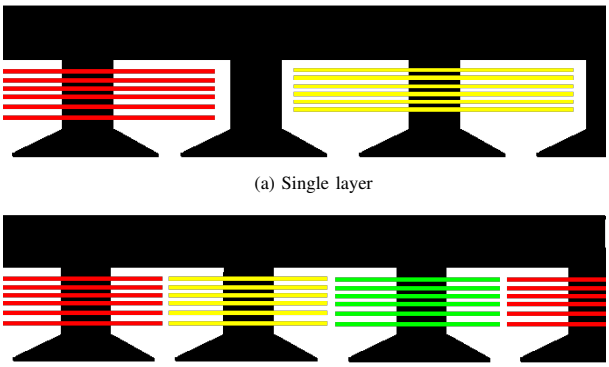

(a) Single layer

(b) Double layer

Figure 2: Layers in concentrated windings

II. PM MACHINERY FUNDAMENTALS AND THEORETICAL EQUATIONS

A. Winding configuration

Conventional winding layouts can be categorised in two main categories: concentrated and distributed windings. Although the term ”concentrated winding” have traditionally been used to explain windings with one slot per pole per phase, it is common to also use the term to explain windings that are ”non-overlapping”, ”fractional slot” or ”tooth” [9]. Traditionally, in three-phase AC electric machinery, the distributed winding is the popular configuration of the two types. This is because it has long been believed that the concentrated winding design could not supply comparable torque, and sinusoidally shaped back emf. This was changed in the beginning of the 21st century when Cros and Viarouge [10], and Magnussen and Sadarangani [11] showed that it was possible to generate a sinusoidal back EMF with concentrated winding with the use of fractional slot winding. Figure 1 show the basic concept of the two types.
Concentrated windings can be categorised in to two subcategories. Single-layer and double-layer winding. As seen in figure 2, the single layer (SL) winding has a coil wound on every other tooth, and in the double layer (DL) there is a coil wound around every other tooth. Having a double layer CW implies shorter, or more compact end windings, and more manoeuvrable coils. However, this also implies the need for radial teeth, instead of parallel teeth which can eliminate the opportunity for pre-fabricated coils. The SL layer also provides inherently good fault tolerance as the coils are mechanically separated from each other.

B. Slot/pole combinations

There is a lot of slot/pole combinations available and that are in commercial use and almost any design with a slotted stator and a random number of windings will produce a torque [3]. Focusing on concentrated windings effectively reduced construction costs, as previously mentioned, since the coils can be manufactured prior to the assembly. In the decision of what slot/pole combination to choose, there are some conventions that apply: [15]

- The number of poles need to be an even number
- The number of pole pairs cannot be a multiple of the number of phases
- If a double layer winding is used the number of poles can not be equal to the number of phases
- If a single layer winding is used the number of poles can not be equal to the number of phases times two

To describe different machines, the parameter q is often used:

$$q = \frac{N_s}{N_{ph} N_p} \tag{1}$$

It states that q equals the number of slots per pole per phase. Machines with a q equal to an integer (e.g: 1, 2, 3...) is said to have a *integral slot winding*. If not, the machine is said to have a *fractional slot winding*.

C. Winding factor

Another important parameter to consider is winding factor, k_w. The winding factor can be calculated in several ways [9], [15], [18]. Equation (2) shows one example of calculating the winding factor using the sum of emf phasors.

$$k_w = \frac{1}{n_l N_s/3} \sum_{i=1}^{n_l N_s/3} \overrightarrow{E_i} \tag{2}$$

[9], where n_l is the number of layers, N_s is the number of slots, $\overrightarrow{E_i}$ is the EMF phasor and i is the slot number of an arbitrary phase.

This fundamental winding factor, k_{w1} gives the peak emf compared to when having a full utilisation of the copper in the winding. One would ask why someone would sacrifice peak emf and its torque-providing ability. This sacrifice (i.e having a $k_w < 1$) is often justified by having a more sinusoidal shaped induced emf, and avoiding cogging torque.

k_w can be split into two contributing factors: the distribution factor (k_d) and the coil pitch factor (k_p):

$$k_w = k_d k_p \tag{3}$$

The distribution factor tells us how the resulting peak emf differs if one would have a concentrated, full pitch coil. When having a distributed, overlapping winding, the total induced

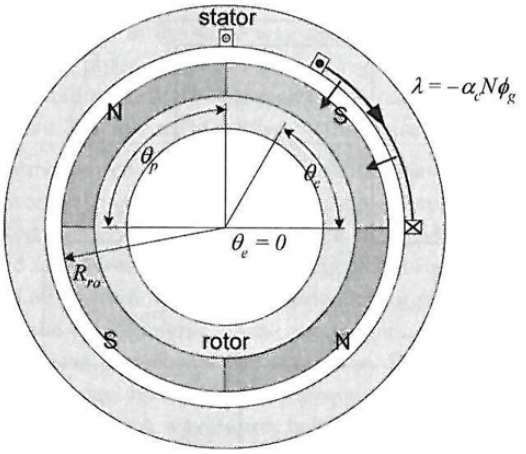

Figure 3: Fractional pitch coil [3]

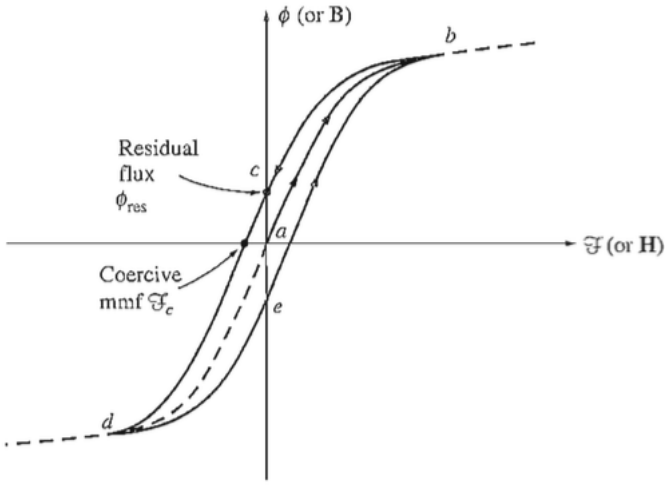

Figure 4: Hysteresis loop for a ferromagnetic material [1]

emf is reduced due to the fact that not all of the copper in the coil experiences the same flux at the same time. Thus in concentrated windings where the number of poles are close to the number of slots, the distribution factor is (almost) equal to 1.

The coil pitch factor (k_p) is a measurement of the coil width related to the pole width. For an example, having a full pitch coil which spans 180°E, the coil pitch factor is equal to 1. Having a coil that spans less than 180°E is often termed a *fractional pitch coil*. In [15], Skaar et. al presented a method for calculating winding factor, and the two contributing factors, without the need to do a winding layout analysis. The method is restated in appendix C. However, in that method it assumed that all the teeth are evenly distributed. Changing the width of the teeth, shifts the slot placement with respect to the pole and thus changing the winding factor. A method to calculate the winding factor that incorporated unequal teeth widths was suggested in the work of Germishuizen and Kamper in [18]. They showed that having a SL CW provides a flexibility in the choice of winding factor. The width of the coil teeth can then be varied to accommodate a wide range of performances. The method from [18] is restated in appendix D.

D. Slot and tooth design

In [16], J. Richnow et. al investigates the effect of absence of tooth shoes in order to facilitate a pre-wound coil manufacturing process. Absence of tooth shoes will in most cases effect the performance of the machine, especially the torque characteristics (cogging, ripple and avg. nominal torque). This was what Richnow et al concluded in their paper, although the effect could be compensated for, with widening the teeth. Since this effectively reduces the slot area, a compromise must be made, either accepting a lower torque performance, or making the overall diameter of the machine larger to make room for windings in the slots. Investigation on implementing cavities on the edge of the teeth where done, but it showed little effect on torque performance, however reducing the ripple to some extent [16].

In the work of Ishak et. al in [17], it was concluded that having unequal tooth widths for SL CW can improve the performance of PM machines. They verified that it is possible to reduce the width of these teeth without causing saturation or limiting the performance of the machine.

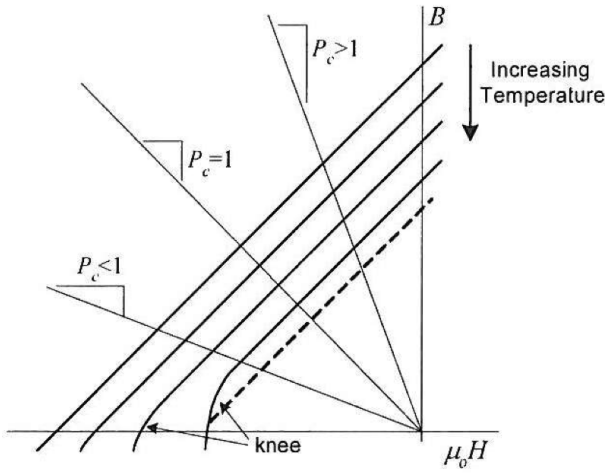

Figure 5: Demagnetization curve for different temperatures [3]

E. Ferromagnetic materials and permanent magnets

Magnetic material is often characterised by their hysteresis cycle. The hysteresis cycle describes the relation between the magnetic field strength $\overrightarrow{H}$ and the magnetic field density $\overrightarrow{B}$ when an alternating field is applied to the material. Figure 4 reflects the nonlinear property of the material. Given a linear material, equation (4) can be considered a linear function, and its corresponding hysteresis cycle would be described by

$$\overrightarrow{B} = \mu \overrightarrow{H} \tag{4}$$

with a constant μ.

Nevertheless, most of the materials in a PM machine are anisotropic and non-linear, varying with both temperature and frequency [5]. The corresponding hysteresis loop, often termed BH-curve would resemble the curves presented in figure 4.

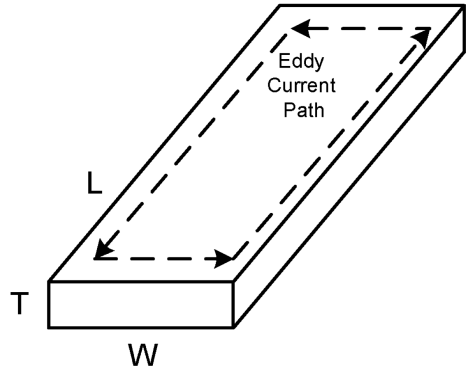

Figure 6: Eddy current path in magnets [19]

An important subject to consider when designing a PM machine is the magnetisation curve of the permanent magnets. It tells us at what operating range it is safe to operate the magnets without risking irreversible demagnetisation. Figure 5 shows the second quadrant of a typical BH curve for a permanent magnet. As depicted, there is a "knee" in the magnetisation curve where the magnet is in risk of irreversible demagnetisation. This would result in permanently reduced performance of the magnet. To prevent this from happening, the operating range of a permanent magnet is at a permeance coefficient, P_c, usually around 4. During operation the field density versus field strength will oscillate around the initial operating point in small circles close to the magnetising curve. This movement is approximately linear along the line described by equation 5. [3]

$$B_m = B_r + \mu_R \mu_0 H_m \tag{5}$$

F. Permanent magnet modelling

Permanent magnet modelling is an essential part of PM machine design. In order to determine, or ball-park parameters it is necessary to do calculations on air gap length and magnet length. Given that the magnetic field strength H_m is dependent on the magnet length, and that the magnetic field density is dependent on the magnetic field strength from the magnets, the magnet length plays an important part of what permeance coefficient the machine is operating on. This can also bee seen from equation 5. The process of determining the magnet length is inspired by the work of Lomheim in 2013, where he analysed an axial flux-machines.

The average air gap flux density in an electrical machine is given by [8]:

$$B_g = \frac{\tau_m \hat{B}_g}{\tau_p} = \alpha_p \hat{B}_g \tag{6}$$

where $\hat{B}_g$ it the peak air gap flux density, τ_p is the pole-sector in radians, α_p is the magnet pitch to pole pitch ratio. Further we have:

$$\hat{B}_g = \frac{B_r}{1 + \frac{g}{l_m}\frac{A_m}{A_g}} \tag{7}$$

Where , B_r is the magnet remanence flux density, g is the air gap lenght, A_m and A_g is the magnet and air gap area respectively and l_m is the magnet length. The air gap area can be calculated:

$$A_g = R_{iron} \tau_p r L \tag{8}$$

Where R_{iron} is the tooth width to slot-opening width ratio given by

$$R_{iron} = \frac{W_t}{W_{so} + W_t} \tag{9}$$

Where W_t and W_s is the tooth width and slot opening width respectively.

The torque developed by a single conductor experiencing a magnetic field is given by:

$$T = rBIL \tag{10}$$

where r is the radius, B is the magnetic flux density, I is the conductor current and L is the conductor length perpendicular to the direction of the flux path. This can be rearranged to [8]:

$$T_{tot} = \frac{3}{2} k_w N_s B_g N I L \tag{11}$$

where, k_w is the winding factor, N_s is the number of slots, B_g is the average air gap flux density. Further, assuming minimal loading, $\theta = \frac{\pi}{6} \Rightarrow I = 2\sqrt{2} I_a \cos(\frac{\pi}{6})$, [8] the expression for air gap flux density can be written:

$$B_g = \frac{T_{tot}}{\frac{3}{2} k_w N_s r N 2\sqrt{2} I_a \cos(\frac{\pi}{6})} \tag{12}$$

Equations 6 to 12 can be used to calculate the required magnet length to achieve a desired air gap flux density.

$$l_m = \frac{g}{\alpha_p \frac{B_r}{B_g} - 1} \frac{\alpha_p}{R_{iron}} \tag{13}$$

G. Core losses

There are two types of core losses present in a machine:

- Hysteresis losses
- Eddy current losses

and they occur mainly two places in an IPM machine:

- Magnets
- Stator and rotor iron

As depicted in figure 4, there is a difference in the direction of the field strength when the material previously have experienced a positive mmf compared to a negative mmf. This dependence on the preceding flux history and the resulting failure to retrace flux paths is called hysteresis [1], and is the source of hysteresis losses.

Magnet losses: Rare earth permanent magnets like neodymium magnets have a low resistivity making them highly exposed to induced eddy currents. In this thesis there will be an evaluation of the magnet losses caused by eddy currents in the magnets. These losses causes heating of the magnets, which is highly undesirable since it changes the magnetisation curve of the magnet and can cause irreversible demagnetisation.

An analytical method for calculating magnet losses is given in appendix A

The most common way to decrease eddy current losses in both magnets and stator and rotor iron is to decrease the conductivity of the materials. In the stator and rotor iron it

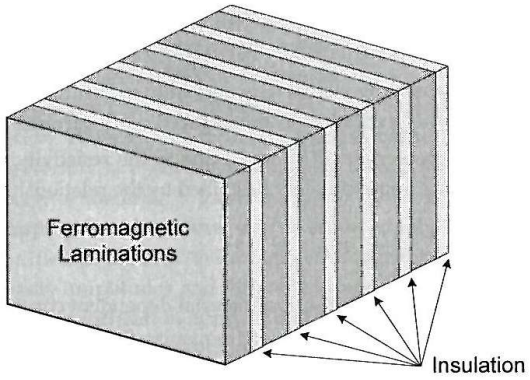

Figure 7: Core laminations for increased efficiency [3]

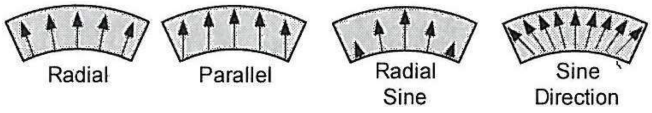

Figure 8: Magnetisation profiles [3]

is common to introduce silicon to the material to achieve this. Additionally it is possible, and very common, to laminate the material. The lamination material is a high resistance and non-magnetic material, and is thus it necessary to orient the laminations parallel to the flux lines. [3].

H. Magnetisation profiles

Figure 8 show different ways of orientating the magnetisation of a permanent magnet. The magnetisation profile of a magnet plays a crucial role of the performance of a magnet, and thus PM machinery. Changing the magnetisation profile of the magnet can change the back EMF of a machine, which again effects the torque generation.

I. Flux barriers

To prevent magnetic short circuiting of the magnets and controlling the magnetisation profile of the poles in IPMs, non magnetic flux barriers are introduced. These are located primarily between the poles, but can also be placed within a pole to manipulate both flux paths and saliency of the rotor.

In [7], by Chong et. al, there was a vast study on the saliency of different IPM designs. The flux barrier design was also investigated, and the conclusion was that the flux barriers can to some extent improve the saliency of the rotor.

In [14], Kim et. al researched the effect on different flux barrier design for a hybrid electric vehicle application, optimising for high torque and low torque ripple. They concluded that design c), in figure **??** is the optimal one when not considering demagnetisation of the magnets.

J. Rotor inertia

When considering a machine's dynamic performance, the rotor inertia is a key factor. In order to have a low inertia the size and weight of the rotor is made as low as possible.

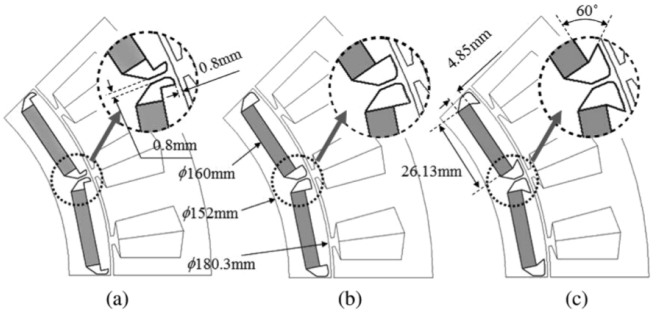

Figure 9: Flux barrier design alternatives [14]

$$J = mr^2 \tag{14}$$

$$= \iint_A \rho r^2 L \, \mathrm{d}A \tag{15}$$

This highly affects the motor torque, so this is something that has to be carefully adjusted in the design process. In order to compare the dynamic performance of different machines the dynamic factor is often used.

$$dynamicfactor = \frac{T_{em}}{J_{rotor}} \tag{16}$$

K. Torque

The general equation for torque in a PM machine is [3]:

$$T = \frac{1}{2} i^2 \frac{dL}{d\theta_e} - \frac{1}{2} \phi_g^2 \frac{dR}{d\theta_e} + Ni \frac{d\phi_g}{d\phi_e} \tag{17}$$

where i is the stator excitation current, L is the mutual inductance between two coils, θ_e is the rotor angle in electrical radians, phi_g is the air gap flux, R is the air gap reluctance and N is the number of turns in a coil.

The two first terms in equation 17 is the torque associated with the varying reluctance. The third term is the torque produced by the magnets. Reluctance torque is often considered parasitic and are unwanted in a machine. This is because it is often preferred to have a smooth torque. The most common parasitic reluctance torque is *cogging torque* [3]:

$$T_{cogg} = -\frac{1}{2} \phi_g^2 \frac{dR}{d\theta_e} \tag{18}$$

Electromagnetic torque expressed by the flux linkages and currents in the direct, and q-axis is given in equation 19, [2].

$$T_{em} = \frac{p}{2} [L_{md} i_{rd} i_{sq} + \underbrace{(L_{sd} - L_{sq}) i_{sd} i_{sq}}_{saliency} - L_{mq} i_{rq} i_{sd}] \tag{19}$$

where L_x is inductance, i_x is current, and the subscript r and s correspond to the rotor and stator values respectively. Subscript d and q represent the direct axis and quadrature axis respectively.

As depicted, there is a saliency term which represent the added usable reluctance torque.

L. Saliency ratio

One of the key benefits of using an interior permanent magnet rotor is, as mentioned in the introduction, the additional reluctance torque component. For this we have a ratio describing the amount of saliency in the rotor [6]:

$$\xi = \frac{L_q}{L_d} \tag{20}$$

where L_q is the quadrature axis inductance, and the L_d is the direct axis inductance.

In a rotor with surface mounted magnets and a cylindrical rotor the saliency ratio would be unity. In [7], Chong and Rahman presented a method for optimising the geometry of the rotor of an IPM to increase the saliency. The results accumulated in a set of design rules for the saliency-optimisation [7]:

- The width and thickness of the magnet must be maximised
- Magnets should not be segmented
- Tip of the flux guides has to be as close as possible to the rotor surface to channel magnet flux flow across the air gap
- Changing the shape of the magnets and having more than a single barrier has little effect on the saliency ratio

M. Total harmonic distortion

The total harmonic distortion, or THD, is a measure of how much a periodic signal differs from a pure sinusoidal signal. A pure sinusoidal signal would have a THD = 0%.

$$THD = \frac{\sqrt{V_2^2 + V_3^2 + V_4^2 \dots}}{V_1} \tag{21}$$

Equation 21 states that the total harmonic distortion of a signal is equal to the ratio of the rms amplitude of the higher harmonic frequencies to the rms amplitude of the fundamental frequency component, V_1.

III. COMSOL Multiphysics as a FEM analysis tool

In this section the main method of building and working with models in COMSOL Multiphysics are reviewed. Much of the work presented here is largely based on, and presented in, the specialisation project, fall 2014 [4].

Finite element analysis tools have, as mentioned in the introduction, become very popular. COMSOL Multiphysics is, as the name indicates, a powerful tool when studying multiple kinds of physics. It has the ability to couple several types of problems in one model where the different elements from different physics can interact with each other.

Solving problems related to rotating electric machines, COMSOL has its own physics-domain related to this type of problem, called *Rotating Machinery, Magnetic*. This is very useful as it lowers the threshold for designers to build, verify and optimise machine designs and ideas.

Finite element method analysis softwares like COMSOL, works in the way that it solves

- Partial Differential Equations (PDEs)

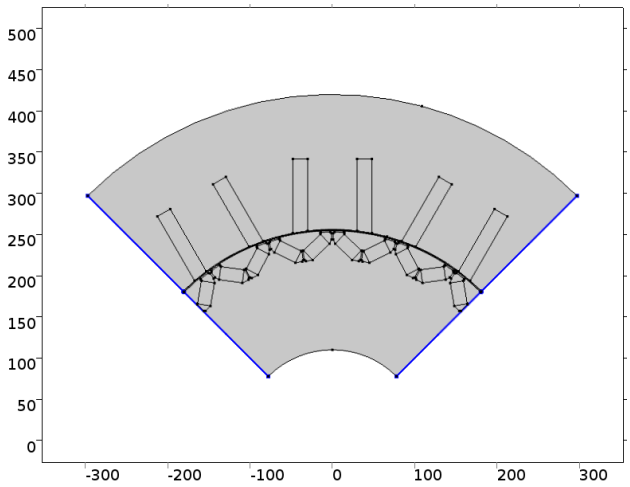

Figure 10: Segmentation of FEM model

- Ordinary Differential Equations (ODEs)
- Algebraic Equations

that are related to the type of problem that you want to solve. It solves the proper equations using a finite element method for a certain number of mesh element corners and intersections. In between these points of the mesh objects it approximates using interpolation.

When using COMSOL to solve a problem consisting of magnetic field and mechanical forces, there are two equations that are especially important:

$$\sigma \frac{\partial \overrightarrow{A}}{\partial t} + \nabla \times (\mu_0^{-1}\mu_r^{-1}(\overrightarrow{B} - \overrightarrow{B_r})) - \sigma \overrightarrow{v} \times \overrightarrow{B} = \overrightarrow{J_e} \tag{22}$$

and

$$\overrightarrow{F} = \int_{\partial\Omega} d\overrightarrow{n} T dS \tag{23}$$

$$\overrightarrow{\tau} = \int_{\partial\Omega} d(\overrightarrow{r} - \overrightarrow{r_0}) \times (\overrightarrow{n}) T dS \tag{24}$$

The PDE given in equation 22 correspond to Ampere's law in the time domain, and the PDEs in equation 23 and 24 corresponds to Maxwell's tensor for force and torque respectively.

A. Geometric Parametrisation

A COMSOL model simulation starts with defining the machine's parameters. If the proper work is done with defining the parameters, the model would be much more flexible and the geometry could easily be changed. This is done for all the models presented in this report, and is especially important for the v-shaped rotor geometry. This geometry requires precise geometric values and a good trigonometrical understanding of the parameters.

In order to get the model solution to converge, it is sometimes useful to avoid sharp edges in the geometry. Having sharp edges can cause some problems as COMSOL interpret them as perfect corners which are infinitely sharp. To solve this problem the "Fillet"-function can be used. This function rounds of the corners. Another possibility is to adjust the mesh (see section about meshing).

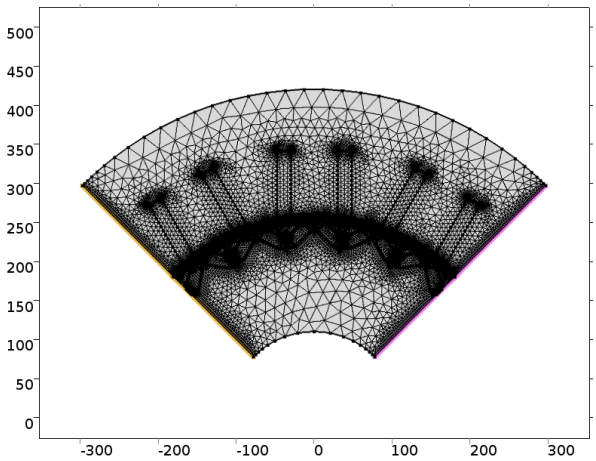

Figure 11: Total mesh

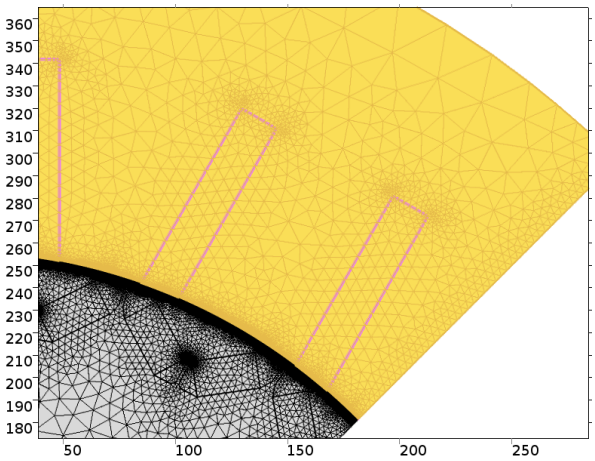

Figure 12: Corner refinement mesh

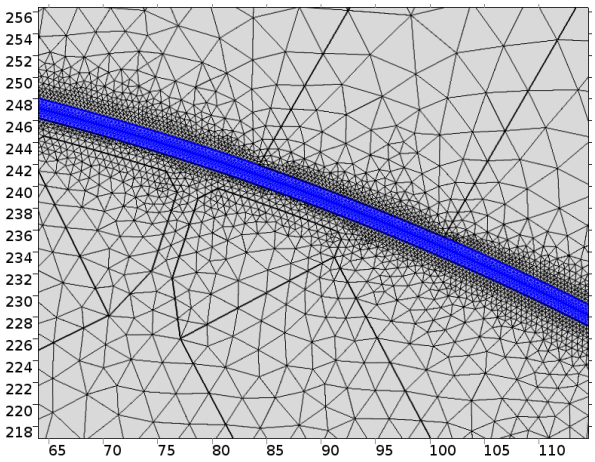

Figure 13: High mesh density in the air gap

Since the model will be simulated in a time dependent study, and there will be a moving part in the model, the model must consists of 2 *unions*. One for the stator and one for the rotor. A union is a collection of domains within a part of the model. The division between the stator and the rotor should be somewhere in the air-gap.

B. Geometric Segmentation

In some slot-pole combinations it is possible to take advantage of magnetic and geometric symmetries. The number of symmetries in a design are defined as:

$$N_{symmetries} = gcd(N_s, \frac{p}{2}) \tag{25}$$

For the 24 slot, 20 pole models largely investigated in this work, the number of symmetries are equal to 4. Thus, it is possible to segment the machine into 4 sectors, only having to do calculations on one of them. In order to make COMSOL evaluate this sector as a part of a larger model the appropriate setting must be done in the *Physics* settings. See section III-F for a closer explanation.

C. Meshing

Appropriate meshing is essential to get an accurate solution of the model. The mesh's job is to divide the model geometry into small, more manageable pieces. Having a fine mesh leads to a more accurate approximation of the solution but takes more time and computational power to solve.

The mesh can consist of several types of elements. For 2D there are:

- Triangle
- Quadrilateral

For 3D:

- Tetrahedal
- Hexahedral
- Triangular prizm
- Pyramid

In the models presented in this report there have been used only triangular mesh-elements. The easiest way to get a relatively decent mesh of the model is to use the *free triangular* option in the mesh settings. This requires however some adjustments to obtain a converging solution.

Firstly there are some areas that need a finer mesh than others. In the coil domains there will, when excited, be a current flowing. Due to the skin effect, the mesh elements must me smaller than the skin depth of the given frequency. In the areas where there will be force calculations, there is also need for a finer mesh. This means that the rotor and air gap domain will be given a finer mesh. In the air gap it is necessary to have up to 8 layers of mesh, in order to get a decent results on the forces in the machine. A high mesh density in the air gap, and thus along the boundary between the stationary and rotating part of the model, is also important since the mesh elements must be aligned with each other across the boundary in order to get a realistic result.

Secondly there should be some corner refinement where there are sharp corners. To help the computation to converge, the best thing is to avoid sharp corners. If that is not feasible a *corner refinement* mesh setting can be added. This is depicted in figure 12. Adding this setting makes a finer mesh around corners to help the solver to a solution that will converge.

Finally there should be an edge mesh on the sector edges. As

mentioned, it is important that the mesh elements are aligned across boundaries. This is also valid for the boundary between sectors. Hence there must be a high-density edge mesh to the far right and left of the model sectors in figure 13

D. Definitions

After the unions are built, the two are defined as an assembly, where the boundary between the components (stator and rotor) is defined as an *identity pair* in the Definitions settings. Here, it is also possible to add or configure equations that is relevant for the problem you would like to solve. The different calculations done on induced back emf, applied current for the different coil domains are designated in these settings.

E. Materials

The different material properties can be loaded from a rich library of materials defined by COMSOL, or it is possible to designate material properties manually. The materials implemented in the models in this report are further presented in section IV. The magnets can be defined material-wise as air since the magnetic properties (besides the remanent flux density) are similar.

F. Physics settings - Rotating Machinery, Magnetic

After the domains have been designated its respective material properties, you need to assign the physical properties of the domains in the model. By default, the boundary properties are given to the exterior boundaries of the model. This will assume magnetic insulation:

$$\overrightarrow{n} \times \overrightarrow{A} = 0 \tag{26}$$

This is an appropriate assumption to make, since the air surrounding the machine have a much lower permeance than the iron in the stator. The initial values for the magnetic vector potential is, also by default, zero. In order to facilitate the segmentation of the machine, it is necessary to implement a *sector symmetry*, and a *periodic condition* on the boundary between the sectors and the different parts of the assembly. Depending on the segmentation, the periodicity must be set to either continuity or antiperiodicity.

The magnetic properties of the magnets and iron are assigned with an "Amperes's Law"-vector potential node. The magnets are assigned the remanent flux density vector ($\overrightarrow{B_r}$). The iron in the stator and rotor is given its appropriate BH-curve-relationship between magnetic field strength and density. The first quadrant of the BH-curve for the iron core material used in this thesis is given in appendix B.

To assign the coil domains their appropriate properties, they are defined with an *external current density* domain setting. This setting allows you to manage the coil direction and excitation current density. This needs to be configured for each direction and phase individually.

It is also possible to define the coils with a *Multi-Turn coil*-vector potential setting. This gives not only easy access to the different coil variables, like current, voltage and power, but also the conductor thickness, resistivity and number of turns. However, this eliminates the functionality to measure the induced EMF for each slot and coil individually. Because of this, the external current density-domain setting was used in this thesis.

IV. Description of modelled machines

It was decided that the work in this thesis should focus on a few specific IPM design philosophies and compare those to a SPM-model to gain understanding on what differs the two types of machines. In this section the process of deciding the parameters for the rotor and stator for the different models are explained. The choices are supported either by the literature research presented in the previous section or by analysis of early analysis results. In order to have a close comparison between the rotor designs, the same stator parameters and winding solution are used in all models. It is believed that this will highlight the differences between the rotor models better, although the optimal performance may not be achieved by the individual combination.

Before starting this work, I was handed a list of performance criteria from SmartMotor. The task was initially to investigate wether these performance criteria could be met with a SL-CW-IPM solution or not. So when designing the machine, the choices was made with the performance criteria in mind. The criteria are given in table I. The machine described is a 840 kW, 20kNm, 400rpm machine which is meant to be used as a steel press. This requires high standards for torque ripple and

Function / Feature / Topic	Required value	Target value
Rated voltage [V]	400 or 690	
Efficiency at rated speed [%]	>95	
Peak stall torque [kNm]		40
Rated speed [rpm]	250	400
Rated torque [kNm]	14	20
Torque ripple[%]		0.5
Max speed at rated current [rpm]	500	800
Rated power[kW]	524	838
Dynamic factor [Nm/(kg · m^2)]	900	1350

Table I: Performance criteria

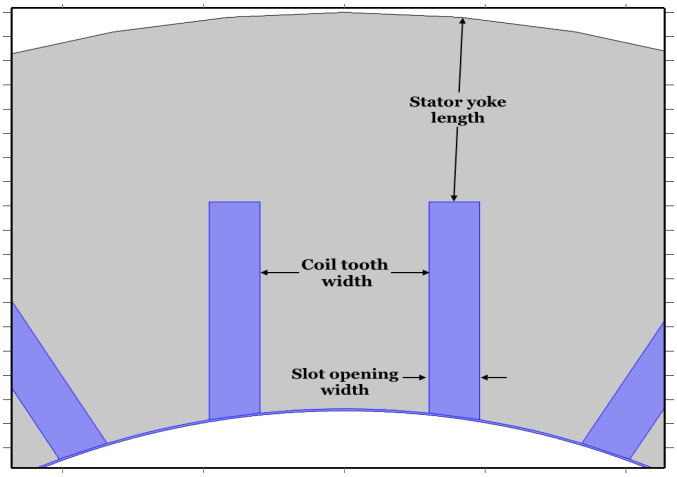

Figure 14: Stator design

dynamic factor as these factors can have a direct effect on the quality of the steel that are being pressed. As this machine is for an industrial customer, there are also high standards for efficiency.

A. Slot and tooth design philosophy

In figure 14 the concept of the stator design and its parameters are depicted. The experienced machine designer might spot the unnecessary long stator length. This is because of the low split ratio of the machine (see table II on stator parameters), which gives the stator inner to outer radius ratio. This was set low so that rotor radius would be low and consequently get a higher dynamic factor. The stator outer diameter is limited to 420 mm, so it was set to that and thus allowing for a long stator yoke length.

To accommodate an automated pre-wound coil manufacturing process, in which the CW mainly has its advantage, a decision to have parallel teeth with no shoes was made. It could be possible to facilitate coil teeth with pole shoes if plug-in teeth where used. This is however costly and leads to a more complex manufacturing process. The parallel teeth forces unequal tooth widths. The effect of having unequal tooth widths have previously been discussed in section II-D.

B. Slot-pole combination

In order to ball-park approximate the number of poles that is appropriate for a given motor parameters, the equation

$$n = \frac{120p}{p} \tag{27}$$

could be used. For a 400 rpm machine with a 50 Hz power supply, this results in a pole number, p, equal to 15. This is an odd number it is therefore not a valid pole number, but it gives a rough estimate of where the pole number should be.

Secondly, if the motor is to be balanced, the number of slots have to be dividable by the number of phases (times two if a SL-CW is used). In table VII in appendix C the fundamental winding factor for different slot-pole combinations are calculated using the method and criteria proposed by Skaar et. al in [15].

For further analysis, the following four slot-pole combinations where considered:

a) 12/10 $\rightarrow k_{w1} = 0.966$
b) 12/14 $\rightarrow k_{w1} = 0.966$
c) 24/20 $\rightarrow k_{w1} = 0.966$
d) 24/22 $\rightarrow k_{w1} = 0.958$

In order to evaluate the different slot/pole combinations, a simple flux density surface plot, where done using COMSOL.

In electric machinery, subharmonics can cause destructive vibrations and noise due to unevenly distributed radial forces. Investigating the plots in figure 15, there are a two-poled subharmonic element in the 12/10, 12/14, and 24/22 combinations. For the 24/20 alternative there are a 4-poled subharmonic element present. Having a higher number of subharmonics means more evenly distributed radial forces.

The low N_s-alternatives, makes more room for having wider teeth in the stator, allowing for more flux to flow through each tooth. They also promotes large slot-areas giving more room for more current-carriers in each slot. However, assuming a SL-CW solution, the coils are wrapped around every other tooth. This can cause trouble in the manufacturing process where the coils are so thick and unmanageable that they can not be bent closely around the coil teeth.

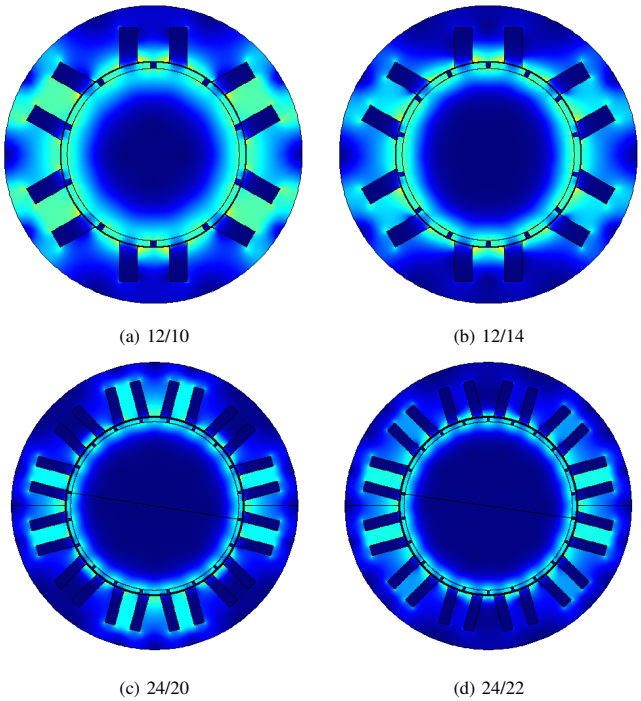

(a) 12/10 (b) 12/14 (c) 24/20 (d) 24/22

Figure 15: Flux density surface plots for different slot/pole combination

Parameter value	Symbol	Value
Stator outer radius [mm]	r_{so}	420
Stator inner radius [mm]	r_{si}	256.2
Split ratio [%]	SR	61.0
Active length [mm]	L	700
Tooth width [mm]	w_t	60
Slot opening width [mm]	w_{so}	18
Stator yoke length [mm]	l_y	75
Slot area [cm^2]	a_{slot}	17.026
Number of turns	N	4

Table II: Stator parameters

For the 24 slot alternatives the possible winding layouts are described in table III. The high winding factor and the 4-poled subharmonic led to decision to focus on the 24 slot 20 pole combination in this thesis. This also facilitated the use of a segmented rotor, since it has more winding symmetries.

		Winding layout
24/20	a)	$RR'\,RR'\,TT'\,TT'\,SS'\,SS'\,RR'\,RR'\,T'T\,T'T\,SS'\,SS'$
	b)	$RR'\,T'T\,SS'\,R'R\,TT'\,S'S\,RR'\,T'T\,SS'\,R'R\,TT'\,S'S$
24/22	a)	$RR'\,RR'\,TT'\,TT'\,SS'\,SS'\,RR'\,RR'\,T'T\,T'T\,SS'\,SS'$

Table III

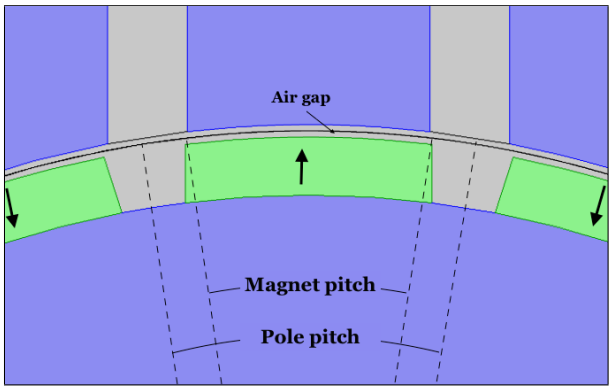

Figure 16: SPM parameter description

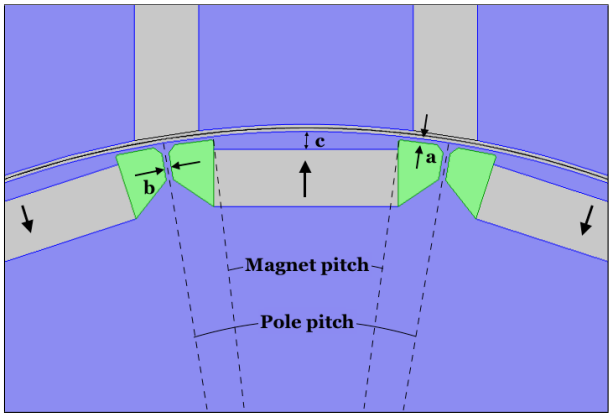

Figure 17: I-shaped IPM parameter description

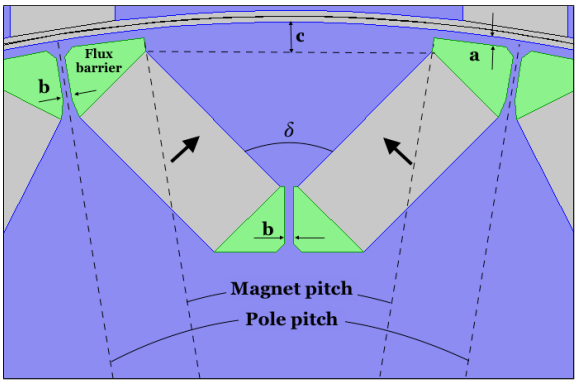

Figure 18: V-shaped IPM parameter description

C. Rotor design

The rotor parameters are given in table IV and their description is showed in figure 16-18. The figures show the main design philosophies applied to the rotor structure of each model. Parameter a, in the IPMs, is defined as the width of the duct between the flux barrier (marked green in figure 17 and 18). This should be as low as possible to minimise the leakage flux and to guide the flux across the air gap. The parameter b, in the IPMs, is defined as the duct width between the poles, and between the magnets within a pole for the v-shaped design. The parameter c, in the IPMs is the magnet depth, defined by the length between the rotor perimeter in the middle of the pole, to the point where there can be drawn a line from the magnet corners closest to the air gap.

Compared to the SPM models, the air gap lengths in the IPM models are reduced. From early investigation there was indications that there was enough leakage flux to reduce the torque performance. To counterweight the hypothesis that the IPM had larger leakage flux, the air gap length was made shorter.

The magnet lengths of the different models where set to be the same. This was to make the comparison as even as possible, so that the effects when performing at the rated torque could be examined.

The rotor radius differs, naturally, between the SPM and IPM models. This is due to the difference in definition of rotor radius in the different types of models. In the SPM model, the rotor radius is defined from the origin to the rotor steel edge, not including the magnet length. This is not the case for the IPM, where the magnets are incorporated in the rotor structure.

The SPM rotor model design was heavily inspired by conventional SPM design, where the magnets are tile shaped, and possesses a parallel magnetisation profile (see figure 8 for description). The magnets in the IPM models are rectangular and also has a parallel magnetisation profile. However, it is believed that the real magnetisation profile of the poles in the IPM model is more dynamic than in the SPM, since the flux direction changes when it crosses the iron between the magnets and the air gap.

The magnet pitch for the different models is defined by the angle between the two corners closest to the air gap, facing the stator. See figures 16-18 for illustration.

The flux barrier designs was inspired by the work presented in [14] by Kim et. al. Their design had an attack angle of 60°towards the centre of the magnets, and meant that this was the optimal design for the i-shaped IPM, when not considering demagnetisation of the magnets, especially at the corners. The 90°attack angle did perform almost the same. To keep the corners less sharp, and thus guaranteeing a more stable FEM simulations the choice was made to keep the attack angle to 90°.

Parameter	Symbol	SPM	IPM	
			I-shaped	V-shaped
No. of poles	N_s	20 mm	20 mm	20 mm
Air gap length	g	3 mm	1.75 mm	1.75 mm
Magnet length	l_m	1.6 mm	1.6 mm	1.6 mm
Rotor radius	r_r	237 mm	254 mm	254 mm
Magnet shape		Tile	Rectangular	Rectangular
PM mag. profile		Parallel	Parallel	Parallel
PM remanence	B_r	1.2 T	1.2 T	1.2 T
Resistivity of magnets	σ		$150 \cdot 10^6 \Omega$ cm	
Pole-to-pole slit	a	-	2mm	2mm
Flux barrier depth	b	-	1mm	1mm
Magnet inset	c	-	5mm	5mm
Core material			Silicon steel NGO N-36	

Table IV: Rotor parameters

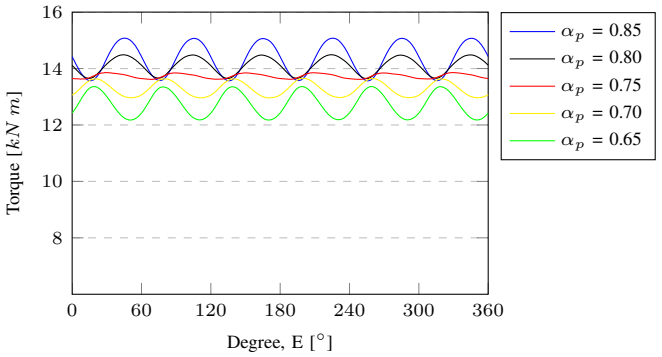

Figure 19: SPM, torque ripple for different α_p

V. Results from FEM analysis

In this section the results from the FEM analysis done with COMSOL Multiphysics are presented. The main performance criteria investigated are:

- Torque characteristics
- Back EMF
- Magnet losses
- Rotor and stator iron saturation

The simulations have been recorded using time-stepping analysis and parametric sweep. The process of getting the final results from the different models, was first to optimise the magnet pole pitch ratio, α_p by performing a parametric sweep, and then reducing the air gap length to do the final, high resolution results, where the areas of interest will be closer evaluated.

A. Torque characteristics

The torque performance of a PM machine is highly dependent on the magnet-pitch to pole-pitch ratio, α_p. To optimise the α_p a parametric sweep was simulated. The time stepping for each parameter was done over a period of 60 electrical degrees. This could be done since the torque ripple had a frequency 6 times as high as the fundamental frequency of the supply, and that it is only required to have a full cycle to get a result on average torque and torque ripple.

For the v-shaped IPM, the magnet angle δ was adjusted to see the effect of flux concentration.

SPM

The result from the parametric sweep done for the SPM is depicted in figure 19. It was calculated with α_p equal to 0.65 to 0.85 with a 0.05 interval. The results show that their is clearly an optimal magnet pitch factor in terms of torque ripple. This optimal magnet pitch factor is approximately 0.75. It should be noted that the direction of the torque ripple is different depending on the magnet pitch factor being higher or lower than the optimal. The average torque production is also increased with increasing α_p. This is due to the increase in magnet area, and thus an increased flux, the higher α_p represents.

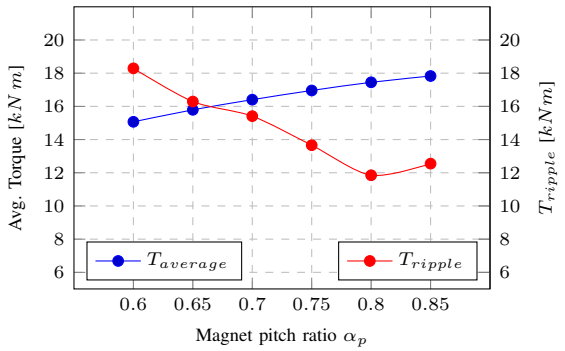

Figure 20: I-shaped IPM torque ripple for different α_p

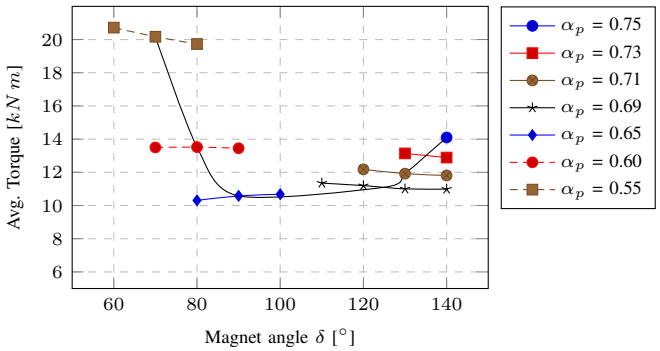

Figure 21: IPMV torque ripple for different δ and α_p

I-shaped IPM

The results from the torque ripple optimisation of the i-shaped IPM model is depicted in figure 20. The same effect that occurred in the SPM model, also happened here. There is a significant optimum magnet pitch factor that minimises the torque ripple and the average torque increases with the increase of α_p. The optimum magnet pitch factor is however changed from the SPM design to this. As where the SPM had an optimum α_p of 0.75, the i-shaped IPM has its optimum between 0.80 and 0.85. The magnet pitch factor that where chosen to investigate further is 0.83.

V-shaped IPM

Figure 21 shows the v-shaped IPM torque ripple performance for different magnet angles and magnet pitch factors.

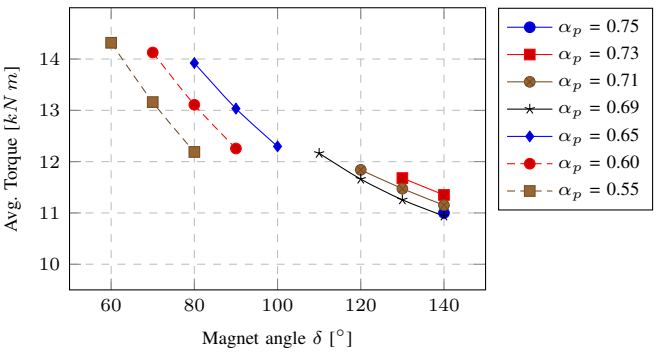

Figure 22: IPMV average torque for different δ and α_p

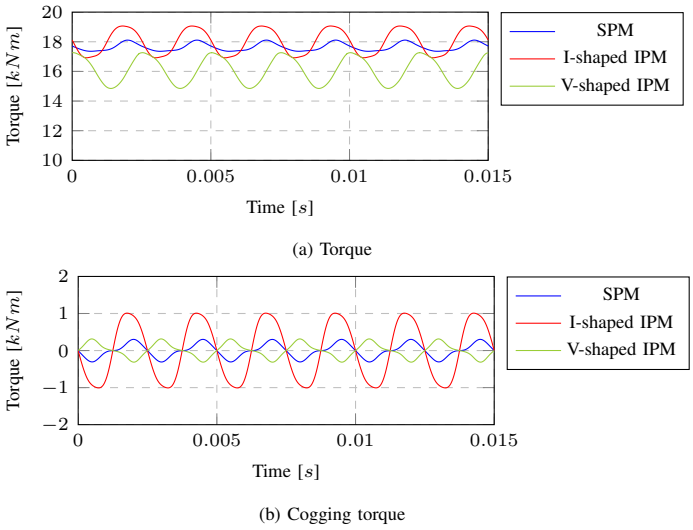

(a) Torque

(b) Cogging torque

Figure 23: Final torque performances

Model	Avg. torque	Torque ripple	Pk-pk cogging torque
SPM	17.645 kNm	4.3 %	0.61 kNm
I-shaped IPM	18.424 kNm	12.9%	2.00 kNm
V-shaped IPM	16.095 kNm	7.22%	0.62 kNm

Table V: Final torque performance

The parametric sweep was done over several magnet angles and magnet pitch factors. Due to the geometrical restrictions in the rotor, the magnet angle possibilities for high magnet pitch factors are limited. The magnet corners facing the neighbouring pole would come in conflict with each other. Similar to the the other designs, there is a certain magnet pole pitch factor that minimises the torque ripple. This optimum is α_p = 0.65. It should be noted that the torque ripple do not seem to be effected by the change of magnet angle.

Figure 22 shows the average torque performance for the different parameter combinations done in the parametric sweep. As the average torque is heavily dependent on the magnet angle δ, the effect of the larger magnet area caused by the increase of α_p is imperceptible.

Final torque results

After the magnet pitch factor optimisation the air gap length was reduced in all of the models to what is described in table IV. The final torque performances is given by the plot in figure 23a. The cogging torque was also calculated and is depicted in figure 23b. The numerical results are given in table V

B. No-load back EMF

The back EMF of the models paints an important picture of how the performance of the machine will be. The harmonic content can tell us something on how we can expect the machine to operate, and what improvements that can be made to the design. The harmonic components are derived from the fast Fourier transform (FFT) solver embedded in COMSOL.

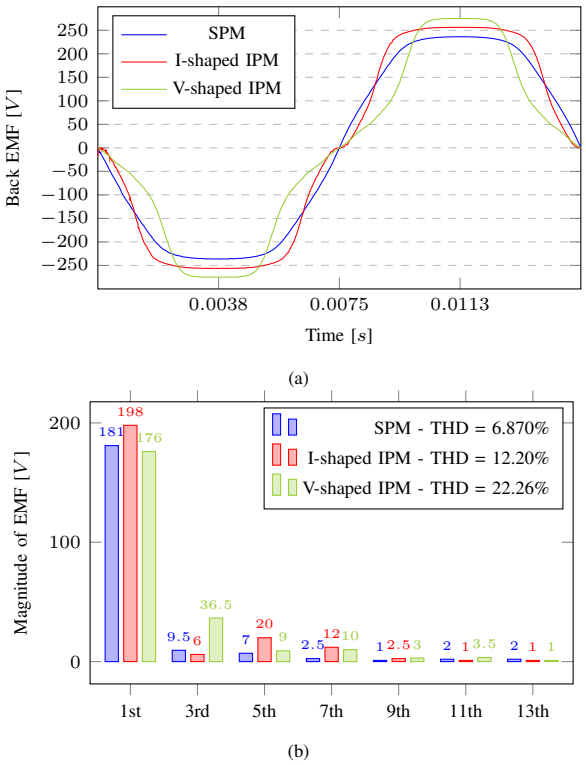

(a)

(b)

Figure 24: Plot and harmonic components of no-load back EMF

SPM: In the back EMF signal of the SPM machine, the results are quite as expected. Since the width of the coil teeth are approximately the same as the pole width, it is a fair to say that the EMF contribution from each slot is approximately the same within a phase. This theory is supported by the results given in figure 24. The peak emf is approximately constant over a time period equal to the α_p of a half electrical cycle (180°,E). The peak value of the back emf is 236 V, and the total harmonic distortion is 6.87%. Considering the higher harmonics, there is no significant component that stands out.

I-shaped IPM: As with the SPM results, the EMF curve of the i-shaped IPM follows the same trend. The magnet pitch factor for this model is 0.83, and thus the time period in which the EMF is at its peak, is longer compared to that of the SPM. It should also be noted that the transition between the zero-range, and full-flux is less smooth than that of the SPM. Even though the magnet pitch factor is larger, there is a small time interval where the EMF is zero. It is believed that this is due to the sudden change of flux linkage and the directional effect caused by the flux barriers. The peak value of the I-shaped IPM back emf is 256 V, and the total harmonic distortion is 12.20%. Considering the harmonics, the 5th and 7th harmonic components are larger than what they should be.

V-shaped IPM: The EMF curve of the v-shaped IPM machine is, as predicted, higher and has a narrower peak than the other models. The effect of flux concentration can bee seen by that the peak EMF is larger, although the magnet pitch factor is lower than in the two other models. The transition

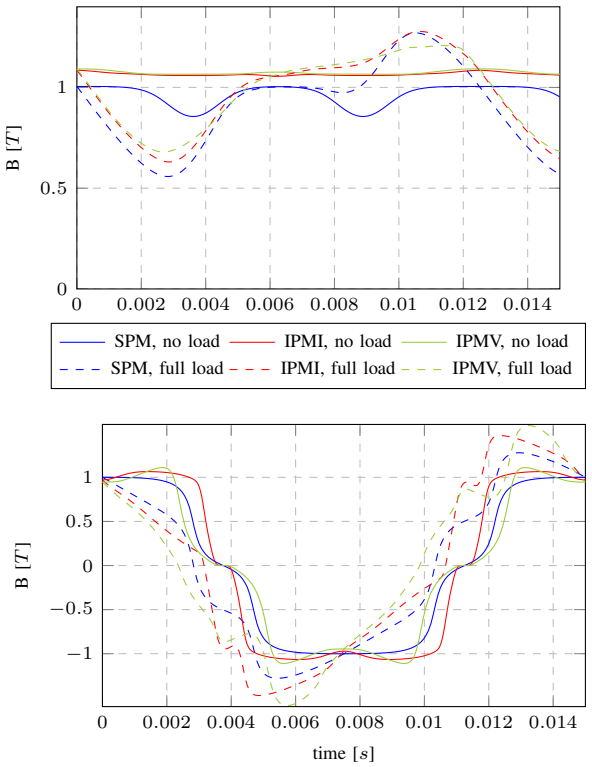

Figure 25: Magnet and air gap flux density in no-load and full load condition

from positive to negative EMF is smoother than in the i-shaped IPM, so it seems like the directional effect of the flux barriers is less in this machine. The peak value of the back EMF is 275 V and the total harmonic distortion is 22.26%. Considering the harmonic components, the 3rd harmonic content in this model is very high compared to the other machines.

C. Air gap and magnet flux density

In figure 25 the different magnet flux densities is plotted over a full electrical cycle. The solid curves, show the magnet flux density under no-load conditions, and the dashed ones show the magnet flux density under loaded conditions. As seen from the figure, the machine that has the most fluctuating magnet flux density under no-load conditions is the SPM machine. It is believed that this is due to the longer air gap length in the SPM machine compared to the other, so that when the pole is crossing a slot opening, the magnet is not able to force the flux across the stator iron. This can also be credited the dynamic magnetisation profile of the IPM machines. Under full load conditions the magnet flux density of all the machines is fluctuating to the approximately same amount, although average level seems to be higher in the IPMs compared to the SPM. The inconsistency of the full load v-shaped IPMs magnet flux density is believed to be caused by saturation of the stator tooth tip iron.

D. Magnet losses

The fluctuation of the magnetic flux density in the magnets combined with the high conductivity of the magnets makes them prone to eddy currents. As mentioned previously, this can cause undesirable heating and lowered efficiency.

		Magnet loss	Loss density	Magnet loss [% of tot. power]
full load	SPM	55.79 kW	4.1859 W/cm^2	7.55%
	I-shaped IPM	73.11 kW	4.8186 W/cm^2	9.58%
	V-shaped IPM	8.81 kW	0.6923 W/cm^2	1.28%
no load	SPM	4.315 kW	0.3238 W/cm^2	0.584%
	I-shaped IPM	279.3 W	0.0191 W/cm^2	0.0366%
	V-shaped IPM	42.82 W	0.0034 W/cm^2	0.0062%

Table VI: Magnet losses caused by eddy currents

In order to investigate magnet losses in the machine, a semi-analytical approach was used. The flux density Fourier components in the magnets was calculated with the FFT solver in COMSOL, and the final calculations where done using the method described in appendix A. The reason for this method was the limitation of computational power and time. According to Tariq et. al **??**, this method provides acceptable accuracy for early, conceptual studies.

The magnet losses for the different machines are given in table VI. As depicted, the v-shaped IPM machine is superior out of the three models. It has a total loss of 8.81 kW, representing a magnet loss density of 0.6923 W/cm^2 and 1.2% of total power. It is believed that this is due the segmentation of the v-shaped magnet since the flux density fluctuation is approximately the same as the rest of the models. This theory is also supported by equation 33 in appendix A, which states that the eddy current losses are proportional to the width of the magnet squared.

E. Magnetic saturation of rotor and stator iron core

Magnetic saturation is caused by the increase of magnetic field strength to the point where the BH curve enters non-linear region. As depicted in figure 29 in appendix B, the magnetic saturation occurs at approximately at $B = 1.5$ for the silicon steel used in these models.

Figures 26-28 show the magnetic flux density surface plots, a magnetic potential contour plot (represented by black, concentric circles) and a surface plot depicting the areas of saturation in the iron. This is represented by a red wireframe, where the data range is from 1.5 T and higher. The plot picture is taken during full load condition at time t = 0. Investigation of the flux plots can reveal flaws in the designs, and areas of improvement. The saturation occurs mainly at the coil tooth tip, the middle of the coil tooth, and at the corner between the coil tooth and the stator yoke. The flux barriers in the IPM does its job by forcing magnetic saturation of the rotor iron between the poles to manipulate the directional property of the magnetisation profile.

VI. Discussion

Torque characteristics: Seen through the critical eyes of industrial standards the results from the machines tested in this thesis is not optimal at all. The levels of torque ripple are well above tolerant levels and would not be up to par with industrial standards. According to the machine performance criteria for

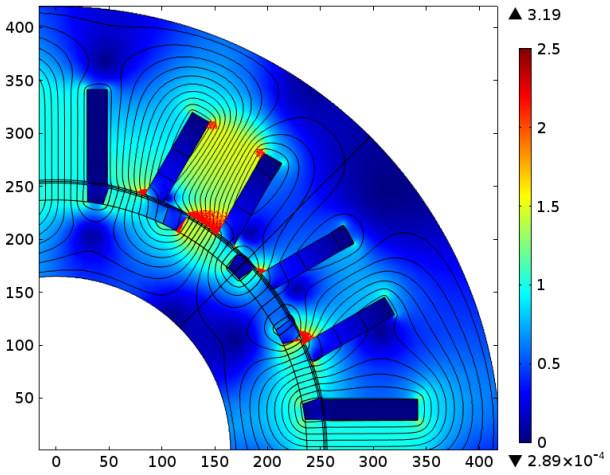

Figure 26: Flux plot of surface mounted rotor

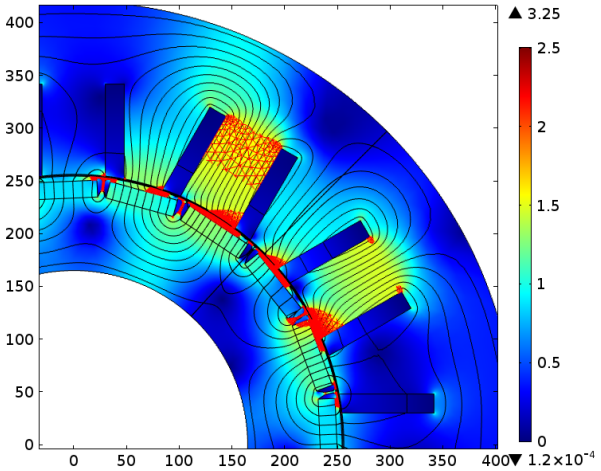

Figure 27: Flux plot of i-shaped IPM rotor

these models, the torque ripple is up to 25 times above the accepted values. In order to do get a more industrial-standard performance out of the machines the machine parameters should be more closely investigated analytically prior to the FEM-analysis. Some of the design concept's advantages and disadvantages are however demonstrated, and it is possible to see the outline of important qualities of the IPM machine.

As stated in the previous section, there is a optimal magnet pitch factor for each design in terms of minimising torque ripple. For the different designs this was α_p = 0.75, α_p = 0.83 and α_p = 0.65 for the SPM, i-shaped IPM and v-shaped IPM models respectively. This indicate that the IPM solution can offer different magnetisation profile, and that the magnet pitch factor must be optimised for different designs accordingly.

The torque ripple results from the v-shaped IPM design show that changing the magnet angle,δ does not effect the torque ripple much. However, when the magnet angle is low enough the torque ripple is effected some by the change of magnet angle. It is believed that this is due to the saturation effects.

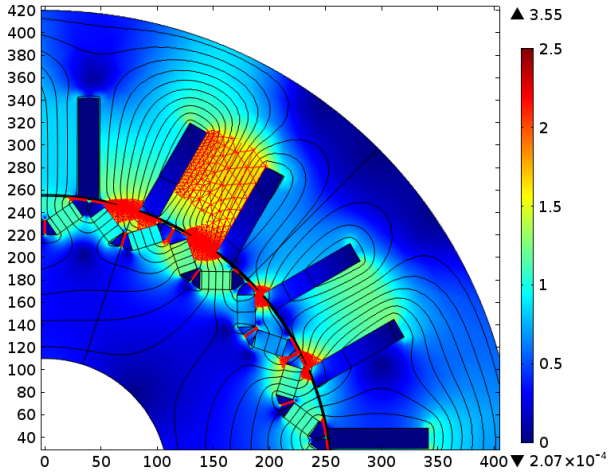

Figure 28: Flux plot of v-shaped IPM rotor

The average torque production of the different machines where 17.645 kNm, 18.424 kNm and 16.095 kNm for the SPM, i-shaped IPM, and v-shaped IPM respectively. This is within acceptable values considering the performance criteria set prior to this work. These results are achieved with a low split ratio of 0.61 and thus exhibits a high dynamic factor.

An increase in the magnet pitch factor resulted in higher average torque for all the machines. This is naturally due to the increase of magnet area per pole and thus the increase of flux linkage. The same effect can be observed from the average torque production from the v-shaped magnet design, where a lower magnet angle δ, resulted in an increase of average torque production. This is although achieved without changing the magnet pitch ratio and exemplifies the flexibility this design has to offer.

From the theory and work done prior to this thesis, there should be a saliency component to the torque of the IPMs. From the results it seems like the saliency component vanishes by the saturation of the coil teeth. It could also happen that the saliency of the models in this thesis not where significant enough to make a difference in these results.

Magnet losses: The loss density of in the different models where 4.1859 kW/cm^2, 4.8186 kW/cm^2 and 0.6923 kW/cm^2 for the SPM, i-shaped IPM, and v-shaped IPM models respectively. This indicates that the the interior PM solution itself is not a magnet loss-reduction design, since the losses are not reduced in the i-shaped i-shaped IPM model, compared to the SPM. The results do however demonstrate the effect of segmenting the magnets. The v-shaped magnet consists of two magnet pieces per pole, and is by that inherently segmented. As expected, the losses is just a fraction compared to the other designs. This is most likely due to the fact that the magnet losses are proportional to the width of the magnet squared. The magnet flux density plot, which shows no particularly difference in fluctuation in the two IPM-models, also supports the theory that these results are caused by the magnet segmentation.

The magnet losses are calculated by using a semi-analytic approach where the flux density of the magnets are calculated

with COMSOL. This method is rather unconventional, and the liability of this approach and these results is somewhat uncertain. In order to increase the liability of the results, a more realistic models should be built which includes conductivity of the magnets.

Magnetic saturation of stator and core: The effect of saturation in these results is believed to be prominent. The effect of saturation of the iron would in theory cause lowered performance of the machine. In the v-shaped IPM it is believed that this is the case. There are several of the results that supports this theory: the alarming flux plot image, the irregular magnet flux density plot where the peak is "cut-off", and its poor torque performance despite its flux concentration. To fix this problem, the split ratio could be increased and thus making room for wider teeth. This would most likely effect the dynamic factor of the machine, but gives also room for making a lighter rotor structure to decrease the rotor's moment of inertia. Another possibility is to investigate the design with a shorter air gap combined with shorter magnet length, and less flux concentration.

VII. Conclusion

As mentioned in the introduction, there are great interests in investigating the use of CW in combination with IPM. The hope is that these designs philosophies can complete each other in order to increase the efficiency, performance and manufacturability of the modern PM machine. However, the tradeoffs are not fully discovered and developed. The work done in this thesis highlights and verifies some of the benefits, drawbacks and possibilities these designs have to offer. The IPM philosophy includes an endless range of rotor configurations. This thesis have focused on two simple designs, which is often preferred by the industry.

The anticipation for the IPM-design to have a magnet loss-reducing effect have not been verified by the results presented in this thesis. The IPM results showed to have more or less the same flux density variation under loaded conditions, and hence are equally prone to magnet losses as the SPM design. In the no load condition, however, there seems to be no flux variations of significance, and hence the no-load magnet losses are improved by the IPM design.

The average torque production of the IPM designs investigated in this work have showed to be able to match the level of the SPM.

The torque ripple, however, is significantly higher in the IPM designs. The IPM designs introduces a lot of new variables to the modelling process and by that increases the complexity of the optimisation process. The optimisation of magnet pitch angle was not sufficient to lower the torque ripple to acceptable levels. It is believed that this can be resolved by the flexibility of the single layer concentrated winding, optimisation of the flux barrier design and possibly by the use of pre-fabricated plug-in teeth with pole shoes.

VIII. Suggestions for further work

The work done in this thesis have highlighted several areas of interest considering IPM with CW. As mentioned in the previous section, both design philosophies offer great flexibility and should be able to meet a wide range of requirements. This requires however complex optimisation processes, as it introduces several new variables.

The possibility to optimise the winding factor by widening the coil teeth for a SL CW is interesting as it can increase the torque production produced by the machine and also adjust the torque ripple.

The effect of adjusting the depth of the magnet, i.e how deep the magnets are submerged into the rotor structure should also be investigated. From previous work on IPMs, the results have shown that the areas that are most prone to demagnetisation and magnet losses are the ones closest to the air gap. This could possibly be solved by implementing the magnet deeper into the structure. This will naturally effect the geometric constraints of the magnet size and shape.

Several IPM designs have been suggested in science literature, and an overwhelming amount variations and philosophies are available. The i-shaped and v-shaped models are some of the simpler ones. Keeping in mind that the industry is prone to select simple, and thus cheap, options, a simple solution should be favoured.

For the v-shaped design, there is a possibility to change the magnet angle, and thus offer flux concentration which again leads to higher torque production. To achieve an even higher torque production, an investigation on how the magnet angle effects the saliency of the rotor should be done.

Magnet segmentation have briefly been demonstrated in this thesis by the v-shaped IPM design, which inherently is segmented. It was suggested in [7] that magnet segmentation would reduce the preferable saliency in the machine. This should be investigated further to fully evaluate the trade-off between magnet losses and reduced torque production from reduced saliency.

References

[1] S.J. Chapman, *Electric Machinery Fundamentals, Fifth Edition*, Australia: McGraw-Hill Education, 2012.

[2] N. Mohan, *Advanced Electric Drives, Drives, 2001 Edition*, Minneapolis, USA: MNPERE, 2001.

[3] D Hanselman, *Brushless Permanent Magnet Motor Design, Second Edition* , Maine, USA: Magna Physics Publishing, 2006.

[4] C. Svihus, *"Investigation of Permanent Magnet Synchronous Machines with Interior Magnets for High Dynamics Applications*, Trondheim, Norway: The Norwegian University of Science and Technology, 2014

[5] L. Chong, *"Design of an Interior Permanent Magnet Machine with Concentrated Windings for Field Weakening Applications"*, Sydney, Australia: The University of New South Wales 2008.

[6] L. Chong,R. Dutta, D. Xiao, M. F. Rahman, H. Lovatt,*"Experimental Verification of Open Circuit Parameters of an IPM Machine with Concentrated Windings"*, IEEE Sydney, Australia: The University of New South Wales 2011

[7] L. Chong,R. Dutta, M. F. Rahman,*"Saliency Ratio Optimization in an IPM Machine with Fractional-slot Concentrated Windings"*, IEEE Sydney, Australia: The University of New South Wales 2008

[8] S. Lomheim, *Analysis of a Novel Coil Design for Axial Flux Machine*, Trondheim, Norway: Norwegian University of Science and Technology, 2013.

[9] F. Meier, *"Permanent Magnet Synchronous Machines with Non-Overlapping Concentrated Windings for Low-Speed Direct-Drive Applications"*, Stockholm, Sweden: KTH 2008.

[10] J. Cros and P. Viarouge, *"Synthesis of high performance PM motors with concentrated windings"*, IEEE Quebec, Canada: Laval University 1999

[11] F. Magnussen and C. Sadarangani, *"Winding factors and Joule losses of permanent magnet machines with concentrated windings"*, in *Electric Machines and Drives Conference, IEMDC'03* IEEE International, vol. 1. page 248-253, 2003
[12] P. Zhang, G.Y. Sizov, J. He, D.M. Ionel, N.A.O. Demerdash, *"Calculation of Magnet Losses In Concentrated-Winding Permanent Magnet Synchronous Machines Using a Computationally Efficient - Finite Element Method"*, IEEE Milwaukee, WI, USA: Marquette University 2012
[13] D. Ishak, Z.Q Zhu, D. Howe, emph"Eddy-Current Loss in the Rotor Magnets of Permanent-Magnet Brushless Machines Having a Fractional Number of Slots Per Pole", IEEE Sheffield, UK: The University of Sheffield, 2005
[14] K.C Kim, D.H Koo, J.P. Hong, J. Lee, *"A Study on the Characteristics Due to Pole-Arc to Pole-Pitch Ratio and Saliency to Improve Torque Performance of IPMSM"*, IEEE Seoul, Korea: Hanyang University, 2007
[15] S.E Skaar, Ø. Krøvel, R. Nilssen, *"Distribution, coil-span and winding factors for PM machines with concentrated windings"*, IEEE Trondheim, Norway: Norwegian University of Science and Technology, 2006
[16] J. Richnow, D. Gerling, P. Stenzel, *"Torque Ripple Reduction in Permanent Magnet Synchronous Machines with Concentrated Windings and Pre-Wound Coils "*, 2014 17th International Conference on Electrical Machines and Systems (ICEMS),Oct. 22-25, 2014, Hangzhou, China D-85577 Neubiberg, Germany: Universitaet der Bundeswehr Muenchen
[17] D. Ishak, Z.Q. Zhu, D. Howe, *"Permanent-Magnet Brushless Machines With Unequal Tooth Widths and Similar Slot and Pole Numbers"*, IEEE TRANSACTIONS ON INDUSTRY APPLICATIONS, VOL. 41, NO. 2, MARCH/APRIL 2005 Sheffield, UK: The University of Sheffield
[18] J.J Germischuizen, M.J Kamper *"IPM Traction Machine With Single Layer Non-Overlapping Concentrated Windings"*, IEEE TRANSACTIONS ON INDUSTRY APPLICATIONS, VOL. 45, NO. 4, JULY/AUGUST 2009 p. 1387-1394 Technology and Innovation Department, Loher GmbH, 94099 Ruhstorf, Germany,Department of Electrical and Electronic Engi- neering, Stellenbosch University, Stellenbosch 7602, South Africa
[19] A.R Tariq, C.E. Nino-Baron, E.G Strangas, *"Iron and Magnet Losses and Torque Calculation of Interior Permanent Magnet Synchronous Machines Using Magnetic Equivalent Circuit"*, IEEE TRANSACTIONS ON MAGNETICS, VOL. 46, NO. 12, DECEMBER 2010 p. 4073-4080 East Lansing, Michigan, USA: Michigan State University
[20] A.M El-Refaie, *"Fractional-Slot Concentrated-Windings Synchronous Permanent Magnet Machines: Opportunities and Challenges"*, IEEE TRANSACTIONS ON INDUSTRIAL ELECTRONICS, VOL. 57, NO. 1, JANUARY 2010 p. 107-121 Electrical Machines and Drives Laboratory, General Electric Global Research Center, Niskayuna, NY 12309 USA.

APPENDIX A
METHOD FOR CALCULATING MAGNET LOSSES [19]

In [19], Tariq et. al presents a method for predicting magnet losses was presented. It is originally used in a proposed analytical analysis, based on a magnetic circuit model. In the models presented in this thesis, the magnet flux density is computed from FE analysis, neglecting magnet conductivity. Given the width, W, thickness, T, and length, L, of the magnet and the area, $A = LW$, perpendicular to the magnetic flux lines, the eddy current path is along the length of the magnet. A figure depicting this is given in the Theory section, figure 6. The eddy loops can be considered as two voltage sources so the induced voltage in one magnet can be described as:

$$V = \frac{A}{2}\frac{\mathrm{d}B}{\mathrm{d}t} \tag{28}$$

representing the flux density in Fourier series:

$$\begin{aligned} V &= \frac{A}{2}\frac{\mathrm{d}}{\mathrm{d}t}\sum_{n=1}^{\infty}(C_n\cos(n\omega t) - \theta_n) \\ &= \frac{A\omega}{2}\sum_{n=1}^{\infty}(-nC_n\sin(n\omega t)) \end{aligned} \tag{29}$$

where the rms voltage is:

$$\begin{aligned} V_{rms} &= \sqrt{\frac{1}{2\pi}\int_0^{2\pi} V^2 \mathrm{d}\omega t} \\ &= \sqrt{\frac{A^2\omega^2}{4}\frac{1}{2\pi}\int_0^{2\pi}\sum_{n=1}^{\infty}(n^2C_n^2\sin^2 n\omega t)\omega t} \\ &= \frac{A\omega}{2}\sqrt{\sum_{n=1}^{\infty}\frac{n^2C_n^2}{2}}. \end{aligned} \tag{30}$$

Assuming that the current path occupies half of the cross section area of the magnet, and that the magnet is much longer than wide:

$$A_{path} = \frac{TW}{2} \Rightarrow R_{path} = \rho\frac{4L}{TW}. \tag{31}$$

The current density of the magnets is:

$$J = \frac{I}{A} = \frac{V_{rms}}{R_{path}}\frac{1}{A_{path}} = \frac{V_{rms}}{2\rho L}\sqrt{\sum_{n=1}^{\infty}\frac{n^2C_n^2}{2}} \tag{32}$$

The power loss density of the magnets can then be calculated using:

$$P_e = \rho J^2 = \frac{W^2\pi^2 f^2}{4\rho}\sum_{n=1}^{\infty}\frac{n^2C_n^2}{2} \tag{33}$$

The fourier series components, C_n, is found by using FE simulation and FFT.

APPENDIX B
BH CURVE

The material properties used for the rotor and stator steel laminations are defined by the COMSOL library. The BH-curve, that dictated the relationship between magnetic field strength H and magnetic field flux density, B, is depicted in figure 29.

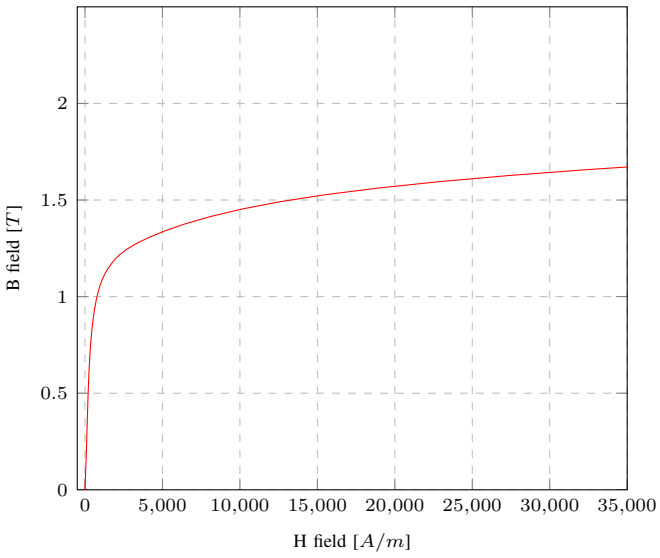

Figure 29: BH curve for silicon steel NGO M-36

APPENDIX C
METHOD FOR CALCULATING WINDING FACTOR, REGARDLESS OF THE WINDING LAYOYT [15]

Considering the equation for q, (eq. 1), and the fact that it is a fraction, the numerator can be named z, and the denominator b. Where z can be found from:

$$z = \frac{N_s}{\gcd(N_s, N_p \cdot N_{ph})} \tag{34}$$

This equation however, is only applicable to DL CW. Making it applicable to SL CW, the parameter $N_c = \frac{N_s}{2}$, which states the number of coils present in the stator, is introduced. The new expression for z for SL CW, is then:

$$z = \frac{N_c}{\gcd(N_c, N_p \cdot N_{ph})} \tag{35}$$

1) Distribution factor: It is assumed that the number of phases, N_{ph}, is equal to three, and the phase spread, σ equal to $60°$. This assumption is appropriate in this work as well.

$$k_d = \frac{\sin(\frac{1}{2}n\sigma)}{z\sin(\frac{n\sigma}{2z})} \tag{36}$$

2) Coil pitch factor: The slot pitch angle is needed to calculate the coil pitch factor.

$$\gamma_s = \frac{\pi N_p}{N_s} = \frac{\pi}{qN_{ph}} \tag{37}$$

The coil span angle, assuming a coil span less than $180°$:

$$\varepsilon = \pi - \gamma_s \tag{38}$$

From this we can calculate the coil pitch factor:

$$k_p = \cos(\frac{1}{2}n\varepsilon) \tag{39}$$

The winding factor is then:

$$k_w = k_p k_d \tag{40}$$

APPENDIX D
METHOD FOR CALCULATING THE WINDING FACTOR, ACCOUNTING FOR IRREGULAR TOOTH WIDTH [18]

Contrary to the method by Skaar, this method is dependent on doing a winding layout before calculating the winding factor. It has its basis in an equation similar to what was given in section II, equation 2. First there has to be introduced some new variables:

$$y_p = \frac{N_s}{p}, \qquad \text{Average coil pitch}$$
$$y_d = \text{int}(y_p) \pm k \begin{cases} k \in N \\ y_p \geq 1 \end{cases}, \qquad \text{Actual coil pitch}$$

The first term above, calculates the average coil pitch, in number of phases. This can be an integer or a fraction. In real machines, the coil pitch must be an integer. The second term calculates the actual coil pitch and adds an adjustment factor, k, which can be adjusted to manipulate the resulting winding factor.

$$k_w = \frac{3}{2N_c} \sum_{i=1}^{\frac{1}{3}N_c} e^{j\phi_{i,p}} + e^{j(\phi_{i,p} - \phi_{\Delta,p})} \tag{41}$$
$$e^{j\phi_{i,p}} = \text{in-going coil side}$$
$$e^{j(\phi_{i,p} - \phi_{\Delta,p})} = \text{Return coil side}$$
$$\phi_{i,p} = \alpha_i \frac{p}{2}\frac{\pi}{180} - \omega_i$$
$$\phi_{\Delta,p} = (k\alpha_p) y_d \frac{p}{2}\frac{\pi}{180}, \qquad 0 < k < y_p$$

ω_i decides the polarity of the coil side. For positive polarity, $\omega_i = 0$, and for negative polarity, $\omega_i = \pi$. For $\phi_{\Delta,p}$, the average angle per slot is,

$$\alpha_p = \frac{2\pi}{N_s} \tag{42}$$

and gives the angle of the return side of the coil.

Ns \ Np	4	6	8	10	12	14	16	18	20	22	24	26	28	30
6	0.866		0.866											
12			0.866	0.966		0.966	0.866							
18					0.866	0.902	0.945		0.945	0.902	0.866			
24							0.866		0.966	0.958		0.958	0.966	
30									0.866	0.874		0.936	0.951	

Table VII: Fundamental winding factor for different slot/pole combinations [15]